



# Measurement of absorption in scattering media using objective laser speckle: application to blood oximetry

GUILLEM CARLES,  LAURENCE BREWER, AND ANDREW ROBERT HARVEY\* 

<sup>1</sup>School of Physics and Astronomy, University of Glasgow, Glasgow G12 8QQ, UK

\*Andy.Harvey@glasgow.ac.uk

**Abstract:** Multi-spectral imaging enables non-invasive sensing of chemical concentrations in biological tissue based on measurement of optical absorption, but invariably in the presence of high levels of scatter. Absorption is normally inferred from measurement of contrast of biological features, such as the vasculature, and so accuracy is degraded by the poorly characterized modulation-transfer function of the imaging optics and overlying tissue. We report how experimental characterization of the spectral variation of the tissue point-spread function and associated objective speckle pattern can be used to characterize the absorption spectrum and chromophore concentration, with a particular emphasis on determination of the ratio of oxygenated to deoxygenated hemoglobin within blood. Absorption measurements are determined purely by the geometry of the experiment, without degradation due to optical aberrations and associated light scatter. The technique offers enhanced and low-cost determination of *in vitro* or *in vivo* chromophore characterizations, including blood-gas analysis.

© 2020 Optical Society of America under the terms of the [OSA Open Access Publishing Agreement](#)

## 1. Introduction

The accurate optical measurement of chemical concentrations in scattering media is important for *in vitro*, *in vivo* and *ex vivo* sensing within biological tissue and fluids and also for industrial monitoring. Chemometrics within tissue includes blood-gas analysis of hemoglobin and quantification of other endogenous compounds such as bilirubin or cytochrome oxidase. Concentration measurements of exogenous compounds is important in medical treatment, including for indocyanine green markers and photosensitizing agents used for photodynamic therapy.

The Beer-Lambert law, in its standard [1] or modified form forms the basis for these measurements [2]. The standard form of the Beer-Lambert law states that the ratio of the transmitted to incident intensities of a collimated beam of light transmitted a distance  $d$  to a nominal ‘detection point’ within a turbid medium is given by

$$\frac{I_t^\lambda}{I_o^\lambda} = e^{-(\mu_a^\lambda + \mu_s^\lambda)d}, \quad (1)$$

where  $\mu_a^\lambda$  and  $\mu_s^\lambda$  are the absorption and scattering coefficients of the medium at wavelength  $\lambda$ . For a turbid medium containing  $N$  species of absorbers

$$\mu_a = \frac{1}{\log_{10}(e)} \sum_{i=1}^N c_i \varepsilon_i^\lambda, \quad (2)$$

where  $c_i$  and  $\varepsilon_i^\lambda$  are the concentration and specific absorption coefficient of species  $i$ . For  $\mu_s^\lambda \ll \mu_a^\lambda$ , the absorbance,  $A^\lambda = \log_{10}(I_o^\lambda/I_t^\lambda)$ , is a linear relation enabling direct determination of multiple  $c_i$  from simple transmission measurements and knowledge of  $\varepsilon_i$ . For most biological tissue and for blood,  $\mu_s^\lambda > \mu_a^\lambda$ , throughout the visible bands and at red and infrared wavelengths

$\mu_s^\lambda \gg \mu_a^\lambda$  [3]. Consequently multiply scattered light is dominant and  $A^\lambda$  varies nonlinearly with  $d$  and  $c_i$ . A useful approximation to linear transmittance can be obtained through the so-called modified Beer-Lambert law [1,4],

$$\frac{I_t^\lambda}{I_o^\lambda} \approx e^{-\mu_a^\lambda d + K}, \quad (3)$$

where  $K$  is a constant determined by scattering processes and the geometry of the sample. Determination of  $c_i$  can then progress through a combination of measurement of  $I_t^\lambda/I_o^\lambda$  and calibration for the chosen geometry. Some form of optical sampling, using beam splitters, may be used to determine  $I_t$  and  $I_o$  in a transmission measurement both *in vitro* or *in vivo*. When measurements are made in reflection however, it is common to infer  $I_t$  and  $I_o$  from the contrast of image features. Such intensity-based measurements are prone to significant uncertainty, which can lead to even larger relative errors in determination of  $c_i$ . For example, in the measurement of the ratio of the relative concentration of vascular oxyhemoglobin in the retina [5–11], or within tissue [12], it is common to infer the ratio  $I_t/I_o$  from the contrast of images of the vasculature. For direct imaging of tissue with high-quality optical instruments, light scattering within the instrument can significantly reduce contrast, even for uncontaminated optics, reducing the validity of the Beer-Lambert law. Contrast can be further reduced to very low levels by scattering due to overlying tissue, although it is possible to account for these effects by incorporation of scattering as a free parameter in a physical model for multispectral image formation of vasculature [12].

Investigators in various fields have reported the determination of  $c$  by analysis of the spatial-frequency characteristics of light scattered or reflected from the sample rather than from simple intensity measurements. The variation in laser speckle size with chlorophyll concentration in fruit has been used to choose the optimal time to harvest fruit [13]. The concentration of *Intralipid* within turbid media and the chromophores hemoglobin, melanin and water have been determined from the variation as a function of spatial frequency of the contrast of diffuse reflectance of spatially modulated light [14]. In these measurements, the reduction in contrast with mean-free path provides information on the chromophore concentration, absorption and scattering coefficients. Spatial-frequency domain contrast has also been used to measure tissue oxygen saturation ( $sO_2$ ) during reconstructive surgery [15]. Another approach is to determine  $c_i$  through measurement of the spatial distribution of the diffuse reflectance [16] when a pencil light beam illuminates the sample. A model can be derived and fitted to measured data to determine absorption and scattering parameters of the tissue. These techniques require sampling of the diffuse reflectance at the tissue surface at various distances from the illumination point and require a non-invasive but contact-based measurement at those locations.

We describe here a non-imaging, lensless technique for determination of  $c$ , which is based on the spatial-frequency spectrum of the objective speckle recorded when laser light is focused onto a turbid medium. In contrast to existing methods, the technique does not require features in the scene, such as blood vessels, to provide contrast and since no image is formed there is no degradation due to optics-induced contrast reduction. It thus offers the possibility of simple and low-cost accurate measurement of optical absorption in scattering media, such as underpins important requirements for *in vitro* and *in vivo* blood-gas analysis [17]. This new measurement technique offers particular advantages for oximetry within the microvascular tissue where capillaries are not easily imaged due to their low contrast and high transparency.

In the next section we discuss how measurement of objective speckle enables determination of absorption in scattering media, in Section 3 we discuss Monte-Carlo simulation of the experiment, and in Section 4 we report experimental validation of the technique for scattering of light from a suspension consisting of *Intralipid* scatterer and nigrosin absorber, and its application to oximetry of blood samples from characterization of the laser speckle. In Section 5 we provide discussions and we conclude in Section 6.

## 2. Speckle-based measurement of absorption in scattering media

Laser light focused onto a turbid medium is scattered into the surrounding volume forming a diffuse extended spot of illumination. In the field of biomedical imaging, this spot is called the tissue point-spread function (tPSF) [18]. The size of the tPSF is dominated by the absorption coefficient,  $\mu_a$ , of the turbid media. For example, in blood, the size of the tPSF is larger in red light than in green due to the lower absorption coefficient for hemoglobin in red light. Measuring the size of the tPSF is therefore an indirect measurement of the absorption coefficient,  $\mu_a$ , of the tissue.

We determine the size of the tPSF by recording the objective speckle pattern on a detector close to the sample as shown in Fig. 1. We illuminate and record in cross-polarized light so as to preferentially detect multiply-scattered light that has been subjected to absorption by propagation through the scattering sample. The rejected co-polarized light is dominated by reflections within the instrument, from the surface of the sample and reflected singly-scattered light, which has not propagated through the sample. For this reason cross-polarized sensing is commonly used to enhance image contrast in biomedical sensing and imaging. In unpolarized light the tPSF is radially symmetric, but for illumination with linearly polarized light, the tPSF in the orthogonal polarization has a characteristic quadrifolium shape, as illustrated in the top right of Fig. 1. It may also be used to attenuate light that has undergone only a single scattering event. The formation of the quadrifolium tPSF can be understood in terms of the angular dependence of the geometrical transformation of polarization associated with just two scattering events: scattering of the incident laser light into the surrounding medium and a second scattering event out of the medium. A similar geometrical effect occurs for double reflection by a corner reflector, where the plane of linear polarization is rotated by twice the angle formed between the linear polarization vector and the roof edge [19]. The quadrifolium is observed only for weak scattering where forward scattering between the two salient scattering events dominates causing only modest depolarization. Nevertheless it is widely observed in scattering from biological media [20], including crossed-polarized illumination of the retina [21], of suspensions of bacteria [22], particles [23] and water droplets in clouds [24]. It is also predicted by Monte-Carlo modelling using Mie-scattering theory [25–28].

In the far field, the spatial-frequency spectrum of the speckle is determined by the spatial autocorrelation of the tPSF [29] and so lower absorption leads to a larger tPSF and a wider spatial-frequency bandwidth in the speckle pattern. The simplicity and compactness of the setup is a clear advantage of the technique, one only needs to ensure that the spatial sampling of the speckle pattern as determined by the pixel pitch satisfies the Nyquist criterion and aliasing is not significant: roughly,  $\lambda z > pW$  where  $z$  is the detector-sample distance,  $p$  is the pixel pitch and  $W$  is the effective size of the tPSF (the autocorrelation of the tPSF does not show a defined cut-off but its rapid decay sets an effective size).

The speckle pattern recorded by a detector illuminated by the light from the tPSF has a speckle size that varies inversely with the size of the tPSF as illustrated in Fig. 1. Absorption within the scattering medium can therefore be determined by characterizing the spatial scale of speckle pattern recorded by the detector. We illustrate the concept for measurement of the tPSF and speckle in Fig. 1 for oximetry of a sample of blood, although the technique is applicable to the measurement of absorption in any scattering medium. We thus infer the width of the tPSF from lensless measurement of the spatial-frequency spectrum of the objective speckle pattern. The tPSF could also be obtained from contact-based measurement [16] or from direct imaging, but several advantages are obtained from speckle-based measurement. Probably the most important advantage is that the approach exhibits zero aberrations and so can be made very compact and with an infinite depth of field, which allows very relaxed manufacturing tolerances, while a compact imaging system requires focusing. This is particularly important for *in vivo* measurements within

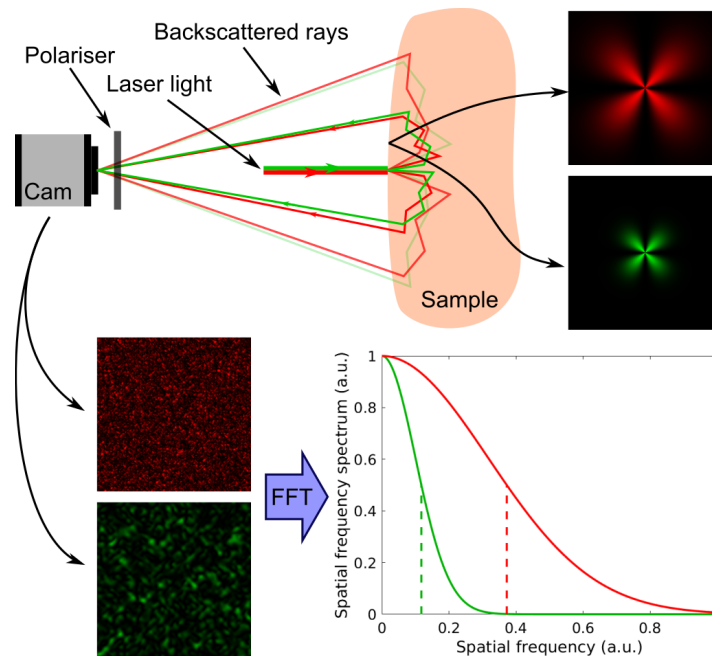


**Fig. 1.** Illustration of the principle of speckle-based measurement of absorption. Polarized laser light is focused to a point (smaller than the tPSF) at the surface of the sample. Rays drawn in red and green exemplify different wavelengths. The quadrifolium tPSF observed under cross polarized light increases in size with reducing absorption coefficient. A sensor (without lens) is placed in the far field to record the objective speckle formed by the backscattered light. Low optical absorption yields a more extended tPSF and a more extended spatial-frequency spectrum for the recorded speckles. Following calibration, the spatial-frequency spectrum of the speckle can thus be used to determine the extent of the tPSF and hence the absorption of the scattering medium.

tissue or the eye, but is also important for *in vitro* measurement within laboratory or clinical instrumentation.

Measurement of the objective speckle pattern at multiple wavelengths offers potential for measurement of, for example, blood oxygenation, without the usual sensitivity to imaging aberrations and contrast reduction associated with imaging of biological structures such as vasculature. Oximetry of vascular blood has been widely applied using calibrated variations in image contrast at two wavelengths [30] or by fitting the free parameters of a physical model to hyper- or multi-spectral images [31,32]. An accurate model of vascular contrast requires calibration of contrast reduction due to light scatter by the instrument, ocular media (in the case of retinal imaging) or by overlying biological tissue and some progress has been made in exploiting the additional data contained within multi-spectral images to calibrate these effects [12]. Our technique for measurement of chromophore concentration (such as is required for oximetry) has no requirement for structure within the object field and so is suitable, for example, for measuring oxygenation in the unresolved capillary bed of tissue. For oximetry of retinal tissue the technique uniquely offers insensitivity to the scattering within the ocular media, which, together with cataract, significantly degrades the contrast of retinal images for older eyes. This could be achieved by imaging the speckle field at the eye pupil when laser illumination is focused at the retina. For *in vitro* measurement of chromophore concentrations, such as underpins blood-gas

analyzers, the technique offers the advantages of a compact lensless measurement technique that is insensitive to contrast reduction of imperfect imaging optics.

The proposed technique is based on the determination of the effective spatial-frequency bandwidth of the recorded speckle pattern, and assumes that it has a monotonic relation with the absorption coefficient. This measurement therefore requires calibration for determination of absorption. This calibration will depend on the complex light paths that scattered light travels to form the tPSF and is in general dependent on sample geometry. In the next section we explore the formation of the tPSF in blood using rigorous polarimetric Monte-Carlo simulation.

### 3. Polarimetric Monte-Carlo simulation of the tissue point-spread function

The size and form of the tPSF, and hence the value of parameter  $\xi$ , is determined by chromophore concentration  $c$ , scattering anisotropy, scattering mean-free path (determined by the size and refractive indices of the scatterers) and by sample geometry. To explore this relation, we used polarization-sensitive Monte-Carlo modelling of light propagation in a scattering medium to simulate the tPSF and associated speckle patterns.

Monte-Carlo modelling is widely used for modelling propagation of unpolarized light in the diffusion regime, but these techniques tend to be not well suited to accurate and holistic modelling of complex systems incorporating both imaging optics and propagation of polarized light in weakly scattering media. We have therefore developed a novel approach of implementing Monte-Carlo simulation of light propagation in a turbid medium using *Zemax OpticStudio* optical-design software [33,34]. This approach uniquely enables rigorously valid Monte-Carlo modelling of complete optical systems, including both propagation in turbid media of arbitrary geometry and through precisely defined lenses of an optical instrument. The heuristic Henyey-Greenstein scattering phase function, which is widely used for Monte-Carlo modelling of light propagation in scattering media, is not valid for scattering of polarized light, and other scattering phase functions are more accurate, including Mie, Gegenbauer kernel and Reynolds-McCormack [35–37]. We have integrated polarization-sensitive Mie-scattering within *Zemax OpticStudio* using a Dynamic-Link Library (DLL) [33,34].

Monte-Carlo simulations were performed for the configuration shown in Fig. 2. Mutually coherent and linearly polarized light rays are focused by a singlet lens onto a slab of turbid medium, with spectral variation in absorption and scattering parameters corresponding to whole blood [38]. Rays are multiply scattered within the volume and a small fraction are subsequently scattered out of the medium and propagate through a polarizer (orthogonal to incident direction of polarization) to the detector. Two lenses, used at infinite conjugate, image the tPSF at the surface of the medium onto an additional pixelated detector in the far field. Therefore, only rays that exit the blood slab with a propagation angle after refraction small enough to enter the aperture of the lenses, were captured at the detector. The boundary conditions at the front and rear interfaces of the blood slab were set to refract and absorb the rays, respectively. Simulations were repeated for each illumination wavelength, using absorption and scattering coefficients for blood [38]. Simulations involved launching of  $4 \times 10^9$  rays for each wavelength, of which approximately  $4.5 \times 10^5$  reached the detector (depending on wavelength). This provided a sufficient number of rays to reproduce the tPSF at the detector. The calculated tPSFs at wavelengths of 594, 604, 612 and 633 nm are shown in Fig. 3(a) and demonstrate the characteristic form of the quadrifolium reported by others [26] and also the expected increase in size with wavelength associated with the decreasing absorption coefficient for wavelengths longer than 586 nm. The simulations assumed Mie scattering, with scatterers of  $6 \mu\text{m}$  in size, and a refractive index a factor 1.052 higher than that of the medium (plasma), giving a scattering anisotropy factor of about  $g = 0.992$ . The density of scatterers was adjusted to result in scattering coefficient reported for blood, that varied only slightly in the wavelength range 594–633 nm, of around 84.7 to 88.6  $\text{mm}^{-1}$  [38].

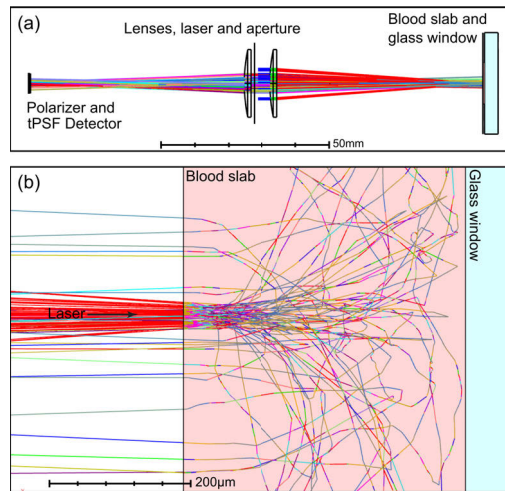


**Fig. 2.** Layout of optics for simulation for recording of the tPSF of a layer of blood sandwiched between glass plates. Modelling was conducted using Mie scattering in *Zemax OpticStudio*. (a) each lens has a focal length of 67 mm and apertures of 6 mm and image the tPSF with unity magnification on a polarized detector; (b) scattering within the 400  $\mu\text{m}$ -thick slab of blood sandwiched between glass windows. Only rays contributing to the tPSF are plotted. The wavelength is 633 nm and rays are color coded for identification purposes.

It is of general interest to understand the formation of the characteristic quadrifolium tPSF. In our simulations of the blood tPSF, we observed that the quadrifolium shape, a characteristic of weak scattering of polarized light, was produced even for large numbers of scattering events. This can be appreciated from the plots in Fig. 3, which show the number of scattering events contributing to the blood quadrifolium tPSF as a function of the annular zones indicated in the inset PSFs. It can be seen that the peak number of scattering events between the key first and last scattering is around 80, but despite this large number, the angular contrast of the quadrifolia are high, indicating that the many, mainly forward-scattering events tend to preserve polarization. The shape of this distribution and to some extent the form of the quadrifolium is also affected by the geometry of the sample; in particular, increasing the thickness of the slab of blood also increases the number of scattering events and reduces the contrast between the dark and bright lobes of the tPSF. It can be appreciated therefore that the form of the tPSF, in particular the degree of angular modulation of the tPSF, may also be used as a means of assessing the scattering characteristics of the turbid sample. In this article, we will focus on scattering within blood, for which the high contrast of the quadrifolium lobes suggests preservation of polarization in the tPSF.

As can be seen from Figs. 3(b) and 3(d), the distribution of rays that form the quadrifolium tPSF per number of scattering events does not significantly change with wavelength. This is expected, because although the absorption coefficient changes significantly with wavelength, the scattering coefficient does not, and the scatterer size, measured in wavelengths, does not change much. However, when considering the integration of the intensity of rays the dependency on wavelength becomes apparent, as can be appreciated from the distributions shown in Figs. 3(c) and 3(e). The number of scattering events of a ray is statistically proportional to the path length it travels within the blood. It also correlates with the distance between the injection and exit points of backscattered rays in the blood, although this depends on sample geometry as well. Rays that exit farther away from the injection point contribute to the higher spatial frequencies of the speckle pattern, and therefore light absorption by blood attenuates these frequencies, as

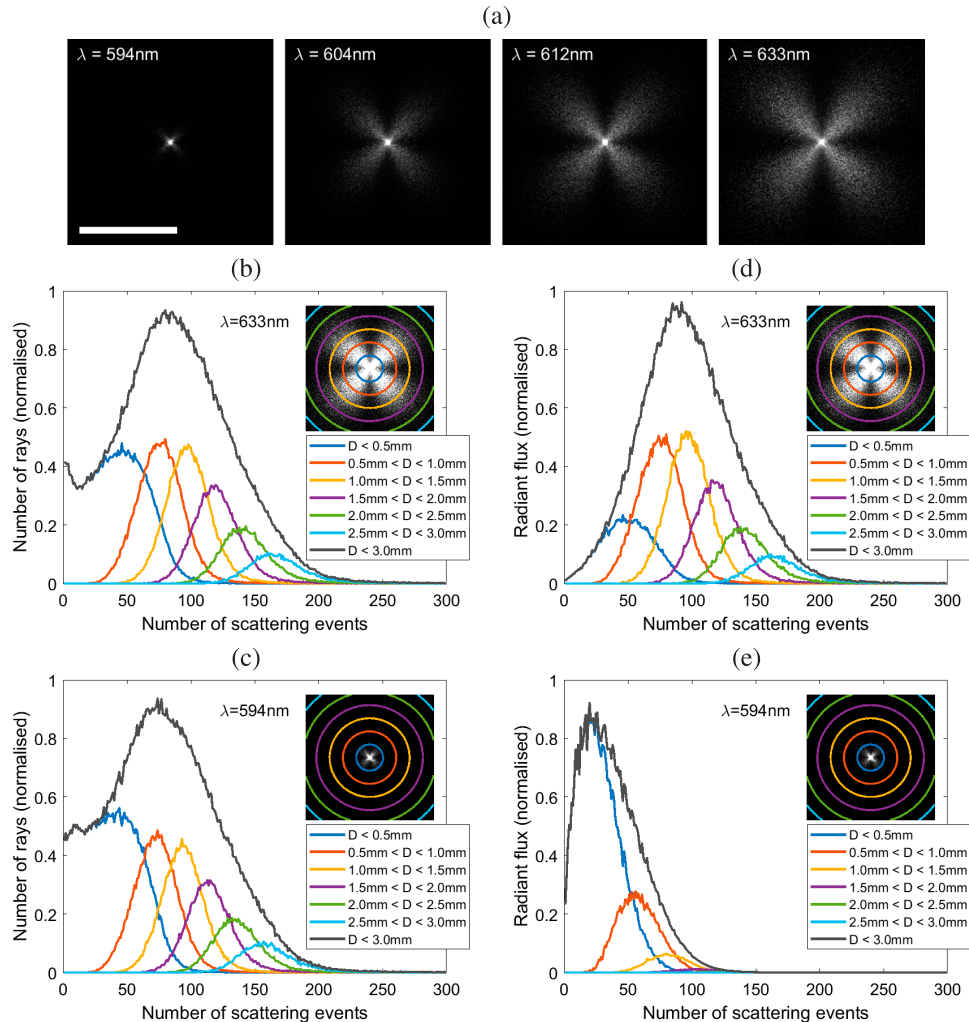


**Fig. 3.** (a) Simulated tPSFs for a  $400\ \mu\text{m}$ -thick layer of whole blood with 100% oxygenation and hematocrit of 45%. The scale bar is 1 mm. (b,c) Plot of the number of rays that reach the detector per number of scattering events undergone, for simulated tPSFs for wavelengths (b) 633nm and (c) 594nm. The various color curves correspond to the concentric annuli containing the last scattering event and indicate that the low depolarization of the scattered light, indicated by the lobe structure, is maintained over 100s of scattering events. (d,e) Radiant flux integrated at the detector (including effect of the polarizer placed in front of the detector) per number of scattering events for wavelengths (d) 633nm and (e) 594; the radiant flux is reduced by the cross-polarization condition and also by light absorption within the blood.

mentioned above. The distributions of the radiant flux per scattering event shown in Figs. 3(c) and 3(e) therefore quantify the effect of light absorption on the spectral content of the speckle pattern.

## 4. Experiments

### 4.1. Methods

Experiments were carried out using the experimental setup illustrated in Fig. 4. Co-aligned tuneable argon-ion and HeNe lasers were used to illuminate the sample plane, providing a selection of illumination wavelengths. The laser light was focused to a diffraction-limited, 25  $\mu\text{m}$  diameter, spot at the sample by an achromatic lens with focal length 100 mm. The far-field cross-polarized speckle pattern was recorded using a lensless detector (Nikon D7000 SLR, 4.8  $\mu\text{m}$  pixel pitch), and a lensed camera (Thorlabs DCC1645C and Nikon 50mm SLR lens) recorded the tPSFs for reference.

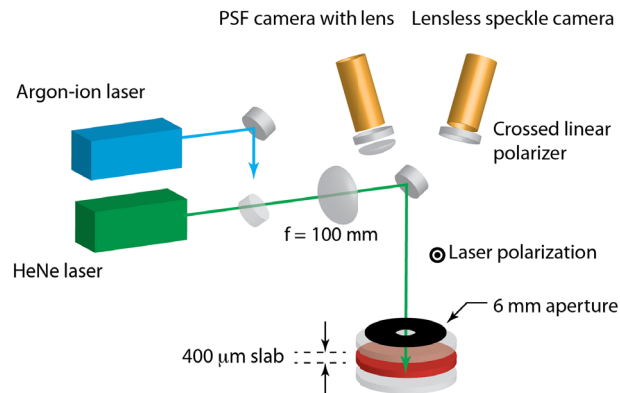


**Fig. 4.** Experimental measurement of tPSF and speckle from a scattering medium held between two 4 mm windows (grey) spaced by 400  $\mu\text{m}$  thick plastic spacers (not shown). A 6 mm diameter felt aperture was used to suppress light reflected and scattered by glass surfaces from reaching the lensless camera. A 100 mm focal length lens focuses light from co-aligned tuneable argon-ion (515nm, 488nm, 458nm) and HeNe lasers (633nm, 612nm, 604nm, 594nm, and 543nm) at the sample.

To characterize the spatial-frequency bandwidth of the speckle pattern, a model fitting is performed. Under given assumptions and approximations it is possible to model the diffuse reflectance from backscattering [16]. However, there is no simple and general analytic form for the quadrifolium tPSF (or indeed any accurate tPSF) from which an analytical form for the spectrum could be derived. We have found however, that a two-dimensional Lorentzian function,

$$L(u, v) = \frac{a}{1 + b_u u^2 + b_v v^2}, \quad (4)$$

yields a useful fit to the spectra of the recorded speckle, where  $(u, v)$  are the spatial frequencies associated with image-plane coordinates  $(x, y)$  respectively, and  $a$ ,  $b_u$  and  $b_v$  are constants to be fitted. (For practical reasons we allow the speckle camera to be tilted with respect to the plane of the sample, projecting a slightly different tPSF scale in  $x$  and  $y$  directions and hence  $b_u \neq b_v$ .)



This simple fitting allows to define a characteristic spatial frequency,

$$\xi = \frac{2}{(b_u b_v)^{1/4}}, \quad (5)$$

which provides a single characterization parameter to represent the size of the tPSF. The parameters  $b_u$  and  $b_v$  are obtained from a least-squares fit of  $L(u, v)$  to the spectra of the recorded speckle.

For the experimental validation of the technique, we prepared a turbid medium with fixed scattering and controlled absorption: a slab of scattering medium, *Intralipid* (Fresenius-Kabi), for various concentrations of an absorber, nigrosin. The *Intralipid* was diluted to 5% by volume using phosphate-buffered saline.

To perform oximetry measurements on blood, we prepared samples using whole defibrinated horse blood with a hematocrit in the range from 38-45%. Blood was partially deoxygenated using sodium dithionite [39] and after allowing 30 minutes to stabilize,  $sO_2$  was sampled using a blood-gas analyser (GEM OPL, Instrumentation Laboratory). The blood sample was held between glass plates, and was inverted before measurement to reduce aggregation of blood cells.

#### 4.2. Experimental validation

To assess the validity of the use of the characteristic spatial frequency,  $\xi$ , to determine absorption within scattering media, speckle patterns were recorded using the *Intralipid* medium through a range of nigrosin concentrations. Results are shown in Fig. 5, which show a linear variation in  $\xi$  with concentration of nigrosin, measured at  $\lambda = 633$  nm. This validates the technique for determination of chromophore concentration. Note that the relation might be determined at any other wavelength and the absorption spectrum of nigrosin would affect this relation accordingly, but we assess here the relation at  $\lambda = 633$  nm.

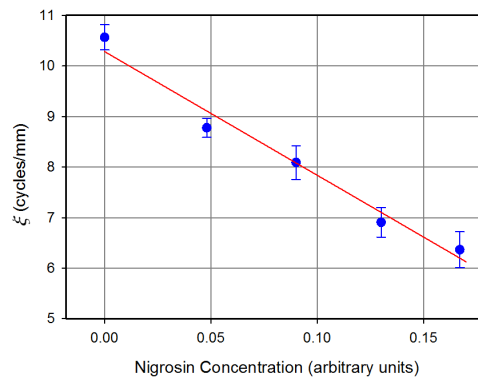


**Fig. 5.** Speckle from *Intralipid* (5% concentration from stock) in a 400  $\mu$ m thick slab with variable concentrations of Nigrosin were recorded at a wavelength of 633nm. The characteristic speckle spatial frequency decreased linearly with increasing concentrations of Nigrosin.

#### 4.3. Blood oximetry using objective speckle

As an example application of the measurement of absorption using objective speckle, we describe here the feasibility of blood oximetry using the experiment shown in Fig. 4. This geometry is pertinent to laboratory measurement within a blood-gas analyser. It is also pertinent to *in vivo* oximetry of the choroid—the highly oxygenated, vascular layer at the back of the eye. Although some rudimentary assessment of relative choroidal oxygenation has been made [40], the absence

of a high-contrast vascular structure means that established vascular-oximetry techniques cannot be used. Our speckle-based technique could therefore provide a route to choroidal oximetry. Laser light at eight wavelengths (633, 612, 604, 594, 543, 515, 488 and 458 nm) from co-aligned HeNe and argon-ion lasers was focused onto horse blood. These wavelengths are a useful selection to sample the variation of the absorption spectrum of hemoglobin as a function of oxygenation, as depicted by the upper plot in Fig. 6.

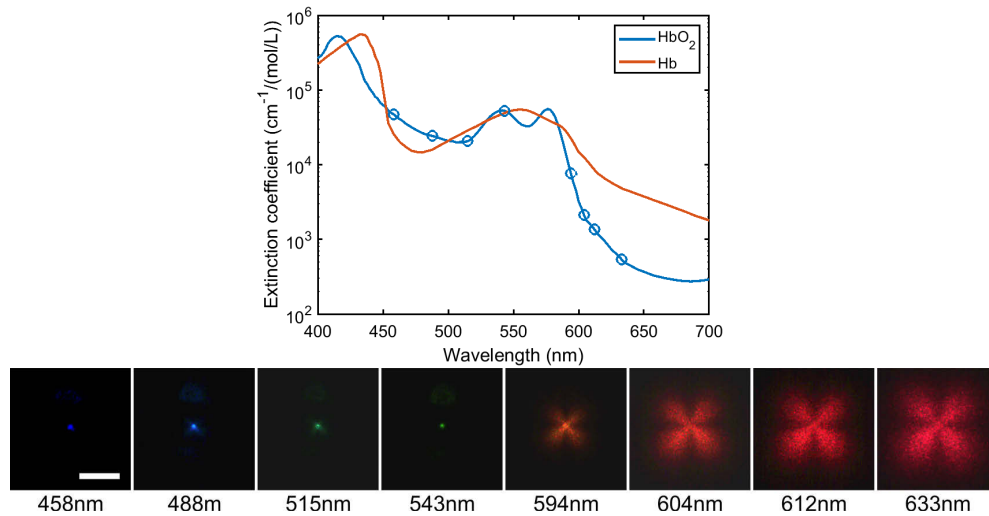


**Fig. 6.** Plot of spectral variation of the molar extinction coefficient of oxygenated and deoxygenated hemoglobin, HbO<sub>2</sub> and HbO (upper) [41] and experimental tPSFs for 400  $\mu\text{m}$  layer of oxygenated horse blood (lower). The transverse dimension of the quadrifolium tPSF varies inversely with absorption coefficient of hemoglobin: from 530  $\text{cm}^{-1}$  at 633 nm to between 20,000 and 50,000  $\text{cm}^{-1}$  for wavelengths in the range 458-543 nm. The scale bar is 1 mm.

Images of the blood-tPSF at eight wavelengths, shown in Fig. 6, exhibit the expected quadrifolium shape. Surprisingly, this seems to be the first report of the measurement of quadrifolium tPSF for blood. As expected, the lateral extent of these tPSFs varies inversely with  $\mu_a$  for hemoglobin (shown in the upper part of Fig. 6) being smaller for wavelengths of 458, 488, 515 and 543 nm for which  $\mu_a$  varies within the range 20,000 and 50,000  $\text{cm}^{-1}$  and then monotonically increases with increasing wavelength up to 633 nm, for which  $\mu_a \approx 530 \text{ cm}^{-1}$ . Typical speckle patterns recorded by the lensless camera are shown in Fig. 7 at each wavelength together with an example two-dimensional spatial-frequency spectrum—for the speckle recorded at 633 nm. The speckle sizes can be seen to vary with the corresponding values of  $\mu_a$ . The variation in the characteristic speckle spatial frequency,  $\xi$ , with wavelength for five values of blood oxygenation is plotted in Fig. 8. The error bars correspond to the standard deviation of  $\xi$  for ten repeated recordings of the speckle pattern.

The greatest variations of  $\xi$  with  $s\text{O}_2$  ( $\Delta\xi / \Delta s\text{O}_2$ ) occur between 604nm and 633nm corresponding to the wavelength range with the greatest differences between the extinction coefficients for oxy- and deoxy-hemoglobin. This is a suitable range for conducting blood oximetry with high sensitivity. The variation of  $\xi$  with  $s\text{O}_2$  at the oxygenation-sensitive wavelength of 633nm is plotted in Fig. 8(right), showing a very linear dependency ( $r^2 = 0.996$ ). The standard deviations of these measurements have an average value of 0.2  $\text{mm}^{-1}$  corresponding to a repeatability in oximetry of 5% and a standard error of our ten measurements of 1.6%. Repeated measurements for improvement of precision is possible since speckle patterns decorrelate quickly due to settling

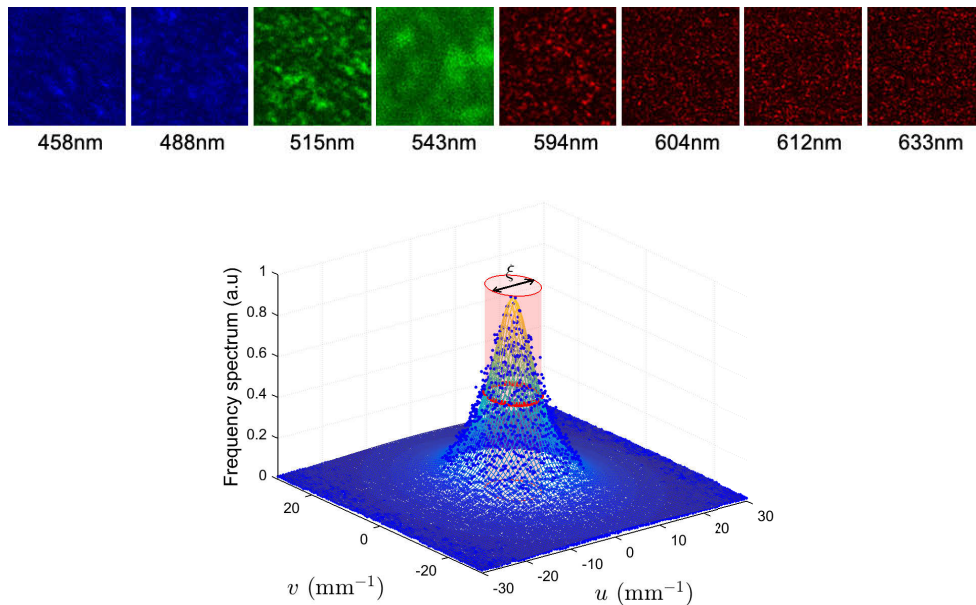


**Fig. 7.** (top) Speckle patterns recorded for all eight wavelengths (images for  $sO_2$  of 100%, pre-processed) and (below) least-squares fit to the spatial-frequency spectrum of the speckle pattern recorded at 633 nm (to enhance visualization purposes the spectrum is down-sampled and smoothed here with a Gaussian filter); the characteristic spatial frequency at the full width at half maximum of the spectrum is plotted in red.

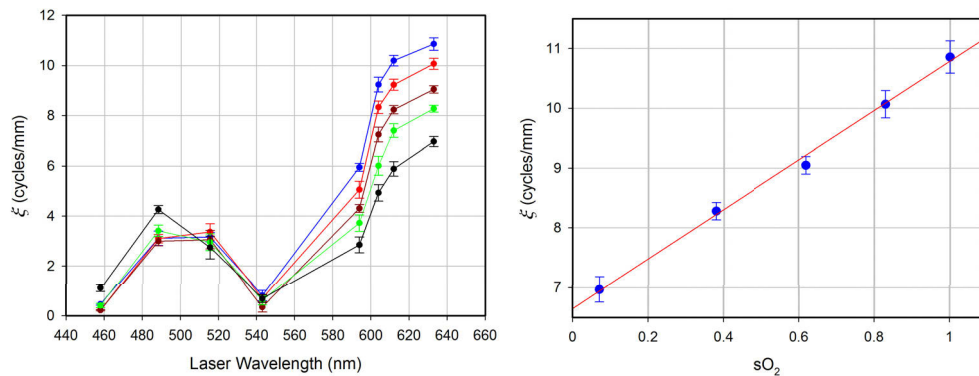


**Fig. 8.** Left: plot of the characteristic spatial frequency of the speckle pattern for oxygen saturation values of 97% (blue), 83% (red), 61% (brown), 39% (green) and 7.1% (black). Right: plot of the characteristic spatial frequency of the speckle pattern at wavelength 633 nm.

of blood cells. Importantly, the speckle pattern needs to be static (which can be ensured by limiting the exposure or illumination time, or by using a pulsed source), as otherwise the fluctuations would temporally average and result in an underestimation of the tPSF width.

## 5. Discussion

We have demonstrated that the spatial-frequency spectrum of objective speckle resulting from point illumination of a scattering medium can be used, following calibration, to determine

chromophore concentration. The measured spectrum is determined only by the measurand and geometry and is therefore insensitive to systematic errors introduced by contrast reduction in the instrumentation, or within the sample, which plague measurement based on the contrast of image features. This is particularly important since these contrast reductions can be very difficult to determine and calibrate particularly for biological measurements [12]. This is pertinent for oximetry in the eye, which has been restricted to oximetry of the retinal vasculature [8,30,32,42] and for which the ocular media can reduce contrast by 50% or more. For this reason absolute vascular oximetry has been elusive. Of particular interest is the feasibility of measurement of blood oxygenation within the capillary bed, for which individual capillaries cannot be resolved. The retinal microvasculature is formed by a collection of capillary blood vessels packed densely enough to approximate a continuous slab of blood. Therefore, measurement of  $sO_2$  *in vivo* may be feasible by imaging objective speckle at the pupil plane of the eye. Note that scattering occurring close to the pupil, such as at the cornea and lens, would cause speckle at a dissimilar spatial frequency to the speckle arising from tPSF and would therefore have little effect on the measured value of  $\xi$ .

We discuss now a comparison between the salient parameters of the measured and simulated tPSF and speckle characteristic frequency  $\xi$ . In Fig. 9 we summarize the variation in  $\xi$  with wavelength for both simulated and experimental data for  $sO_2=97\%$ . It can be observed that while agreement is very good at 458, 543, 594 and 604 nm, simulations predict a value of  $\xi$  at 488 and 515 nm that is a factor of about two smaller than is experimentally observed and at 612 and 633 nm the simulated values are about 10% and 15% too large. Some discrepancy is not unexpected, due to the approximations used in the model: namely, the absorption and scattering parameters used in the Monte-Carlo simulations are for human blood, which has biconcave cells, while the Mie scattering model employed within our Monte-Carlo simulation assumes spherical scatterers with a single size, and the experiments were conducted on horse blood (which has discoid cells). Although an improved match between the model and the experiment is not without interest, the modelling conducted is sufficient to demonstrate that the principles of formation of the quadrifolium tPSF and speckle pattern are well understood.

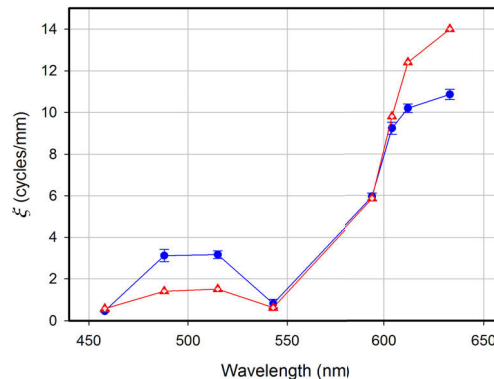


**Fig. 9.** Comparison of characteristic spatial frequency  $\xi$  calculated from simulated speckle (red triangles) and experimentally-recorded speckle (blue circles, taken from Fig. 8 above at an  $sO_2$  of 100%).

As highlighted above, the value of  $\xi$  depends on the value of  $\mu_a$  (which enables determination of blood oxygenation), but also on various other parameters, such as geometry and concentration of scatterers. Our technique is based on the assumption that the size of the tPSF, although dependent on other parameters, is dominated by the absorption coefficient, and therefore calibration can be used to relate the value of  $\xi$  with absorption, as demonstrated. However, other optical

parameters and geometry of the sample will affect such calibration. To explore this, we have conducted Monte-Carlo simulations for a range of scattering parameters and geometries, shown in Fig. 10(a), and also simulations to model the dependence of  $\xi$  on  $\mu_a$  for different selected cases, shown in Fig. 10(b). These simulations confirm a monotonic dependence of  $\xi$  against  $\mu_a$ , suggesting that inversion is feasible given that calibration is available. Of course, employing an incorrect calibration curve would result in errors on the inference of  $\mu_a$  (for example if the sample geometry or optical parameters significantly differ from those used in calibration). However, information from several wavelengths, following calibration, can still be exploited for a more reliable determination of the absolute value of  $\mu_a$ , as is used in pulse oximetry, blood-gas analysis [17] and retinal oximetry [30].

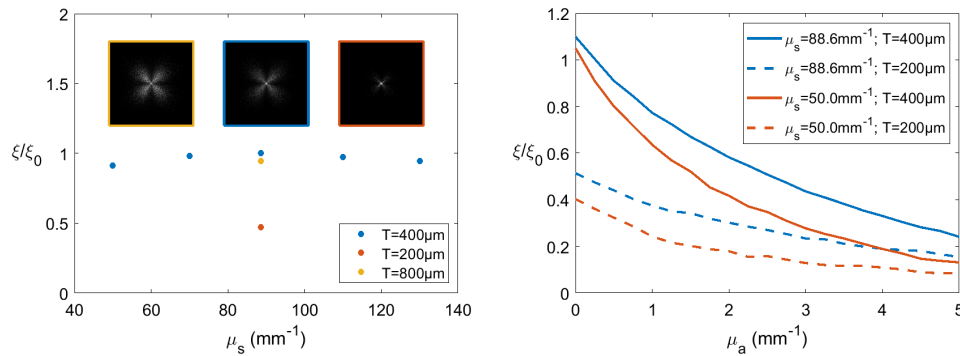


**Fig. 10.** (Left) Dependence of the characteristic speckle spatial frequency  $\xi$  (relative to a reference value  $\xi_0$  corresponding to properties at 633 nm, i.e.  $\mu_a = 0.26$  mm<sup>-1</sup>,  $\mu_s = 88.6$  mm<sup>-1</sup>, and thickness  $T = 400$  nm) on the scattering coefficient and sample geometry; the inset tPSFs are for  $\mu_s = 88.6$  mm<sup>-1</sup>. (Right) Calibration curve, i.e.  $\xi/\xi_0$  against absorption coefficient  $\mu_a$ , for selected cases.

As mentioned, we assume and exploit the fact that the size of the tPSF is dominated by the absorption coefficient. The fact that its size and shape depend also on factors such as sample geometry,  $\mu_s$  or  $g$  (indirectly including scatterers size, shape and concentration), makes their measurement possible by inspecting the shape of the spatial-frequency spectrum of the speckle patterns. Joint determination of  $\mu_a$  and  $\mu_s$  has been demonstrated by measuring the radial dependence of the unpolarized tPSF [16] by model fitting under certain assumptions. Our technique may therefore also be used to determine such parameters, although measurement of the tPSF shape from the spatial-frequency spectrum is more difficult, as the auto-correlation (which we determine) does not uniquely define the tPSF.

## 6. Conclusions

We have described a new technique to measure optical absorption in turbid media, which is insensitive to the imaging aberrations and contrast reductions, which degrade imaging-based measurement. The method involves analysis of the spatial-frequency spectrum of objective laser speckle resulting from point illumination with temporally coherent light. We simulated and experimentally observed a quadrifolium tPSF in a control experiment and also for blood. The control sample demonstrated a linear variation in speckle spatial frequency  $\xi$  with absorption coefficient  $\mu_a$ , demonstrating its suitability for measurement of chromophore concentration. Moreover, we have shown how, for blood, this measure is sensitive to sO<sub>2</sub>, providing a means of performing oximetry in slabs of blood. This paves the way to *in vivo* oximetry in the microvasculature –an important ability that is not currently possible using traditional densitometry-based techniques.

## Funding

Leverhulme Trust (ECF-2016-757); Scottish Funding Council (HR09013).

## Disclosures

The authors declare no conflicts of interest.

## References

1. L. Kocsis, P. Herman, and A. Eke, "The modified Beer–Lambert law revisited," *Phys. Med. Biol.* **51**(5), N91–N98 (2006).
2. J. A. Myers, B. S. Curtis, and W. R. Curtis, "Improving accuracy of cell and chromophore concentration measurements using optical density," *BMC Biophys.* **6**(1), 4 (2013).
3. D. Faber, M. Aalders, E. Mik, B. Hooper, M. van Gemert, and T. van Leeuwen, "Oxygen Saturation-Dependent Absorption and Scattering of Blood," *Phys. Rev. Lett.* **93**(2), 028102 (2004).
4. A. Sassaroli and S. Fantini, "Comment on the modified Beer–Lambert law for scattering media," *Phys. Med. Biol.* **49**(14), N255–N257 (2004).
5. K. Kramer, J. O. Elam, G. A. Saxton, and W. N. Elam, "Influence of oxygen saturation, erythrocyte concentration and optical depth upon the red and near-infrared light transmittance of whole blood," *Am. J. Physiol.* **165**(1), 229–246 (1951).
6. F. C. Delori, "Noninvasive technique for oximetry of blood in retinal vessels," *Appl. Opt.* **27**(6), 1113–1125 (1988).
7. R. Shonat, E. Wachman, W. Niu, A. Koretsky, and D. Farkas, "Near-simultaneous hemoglobin saturation and oxygen tension maps in mouse brain using an aotf microscope," *Biophys. J.* **73**(3), 1223–1231 (1997).
8. S. H. Hardarson, A. Harris, R. A. Karlsson, G. H. Halldorsson, L. Kagemann, E. Rechtman, G. M. Zoega, T. Eysteinnsson, J. A. Benediktsson, A. Thorsteinsson, P. K. Jensen, J. Beach, and E. Stefánsson, "Automatic retinal oximetry," *Invest. Ophthalmol. Visual Sci.* **47**(11), 5011 (2006).
9. L. E. Kagemann, G. Wollstein, M. Wojtkowski, H. Ishikawa, K. A. Townsend, M. L. Gabriele, V. J. Srinivasan, J. G. Fujimoto, and J. S. Schuman, "Spectral oximetry assessed with high-speed ultra-high-resolution optical coherence tomography," *J. Biomed. Opt.* **12**(4), 041212 (2007).
10. B. S. Sorg, M. E. Hardee, N. Agarwal, B. J. Moeller, and M. W. Dewhirst, "Spectral imaging facilitates visualization and measurements of unstable and abnormal microvascular oxygen transport in tumors," *J. Biomed. Opt.* **13**(1), 014026 (2008).
11. T. R. Choudhary, D. Ball, J. Fernandez Ramos, A. I. McNaught, and A. R. Harvey, "Assessment of acute mild hypoxia on retinal oxygen saturation using snapshot retinal oximetry," *Invest. Ophthalmol. Visual Sci.* **54**(12), 7538 (2013).
12. M. A. van der Putten, J. M. Brewer, and A. R. Harvey, "Multispectral oximetry of murine tendon microvasculature with inflammation," *Biomed. Opt. Express* **8**(6), 2896–2905 (2017).
13. R. Nassif, F. Pellen, C. Magné, B. L. Jeune, G. L. Brun, and M. Abboud, "Scattering through fruits during ripening: laser speckle technique correlated to biochemical and fluorescence measurements," *Opt. Express* **20**(21), 23887–23897 (2012).
14. R. B. Saager, D. J. Cuccia, and A. J. Durkin, "Determination of optical properties of turbid media spanning visible and near-infrared regimes via spatially modulated quantitative spectroscopy," *J. Biomed. Opt.* **15**(1), 017012 (2010).
15. J. T. Nguyen, S. J. Lin, A. M. Tobias, S. Gioux, A. Mazhar, D. J. Cuccia, Y. Ashitate, A. Stockdale, R. Oketokoun, N. J. Durr, L. A. Moffitt, A. J. Durkin, B. J. Tromberg, J. V. Frangioni, and B. T. Lee, "A novel pilot study using spatial frequency domain imaging to assess oxygenation of perforator flaps during reconstructive breast surgery," *Ann. Plast. Surg.* **71**(3), 308–315 (2013).
16. T. J. Farrell, M. S. Patterson, and B. Wilson, "A diffusion theory model of spatially resolved, steady-state diffuse reflectance for the noninvasive determination of tissue optical properties in vivo," *Med. Phys.* **19**(4), 879–888 (1992).
17. J. W. Severinghaus, P. Astrup, and J. F. Murray, "Blood gas analysis and critical care medicine," *Am. J. Respir. Crit. Care Med.* **157**(4), S114–S122 (1998).
18. P. van der Zee and D. T. Delpy, "Simulation of the Point Spread Function for Light in Tissue by a Monte Carlo Method," in *Oxygen Transport to Tissue Advances in Experimental Medicine and Biology* vol 215, I. A. Silver and A. Silver, eds. (Springer, Boston, 1987), chap. 9, pp. 179–191.
19. J. Lesurf, *Millimetre-wave Optics, Devices and Systems* (Taylor and Francis, 1990).
20. M. Dogariu and T. Asakura, "Polarization-dependent backscattering patterns from weakly scattering media," *J. Opt.* **24**(6), 271–278 (1993).
21. B. F. Hochheimer and H. A. Kues, "Retinal polarization effects," *Appl. Opt.* **21**(21), 3811–3818 (1982).
22. A. H. Hielscher, J. R. Mourant, and I. J. Bigio, "Influence of particle size and concentration on the diffuse backscattering of polarized light from tissue phantoms and biological cell suspensions," *Appl. Opt.* **36**(1), 125–135 (1997).
23. B. D. Cameron, M. J. Raković, M. Mehrübeoğlu, G. W. Kattawar, S. Rastegar, L. V. Wang, and G. L. Coté, "Measurement and calculation of the two-dimensional backscattering mueller matrix of a turbid medium: errata," *Opt. Lett.* **23**(20), 1630 (1998).

24. S. R. Pal and A. I. Carswell, "Polarization anisotropy in lidar multiple scattering from atmospheric clouds," *Appl. Opt.* **24**(21), 3464–3471 (1985).
25. J. C. Ramella-Roman, S. A. Prahl, and S. L. Jacques, "Three monte carlo programs of polarized light transport into scattering media: part I," *Opt. Express* **13**(12), 4420–4438 (2005).
26. J. C. Ramella-Roman, S. A. Prahl, and S. L. Jacques, "Three monte carlo programs of polarized light transport into scattering media: part II," *Opt. Express* **13**(25), 10392–10405 (2005).
27. M. J. Raković and G. W. Kattawar, "Theoretical analysis of polarization patterns from incoherent backscattering of light," *Appl. Opt.* **37**(15), 3333–3338 (1998).
28. X. Wang and L. V. Wang, "Propagation of polarized light in birefringent turbid media: A monte carlo study," *J. Biomed. Opt.* **7**(3), 279–290 (2002).
29. J. Dainty, "The statistics of speckle patterns," in *Progress in Optics*, vol. 14 E. Wolf, ed. (Elsevier, 1977), pp. 1–46.
30. J. M. Beach, K. J. Schwenzer, S. Srinivas, D. Kim, and J. S. Tiedeman, "Oximetry of retinal vessels by dual-wavelength imaging: calibration and influence of pigmentation," *J. Appl. Physiol.* **86**(2), 748–758 (1999).
31. D. J. Mordant, I. Al-Abboud, G. Muyo, A. Gorman, A. Sallam, P. Ritchie, A. R. Harvey, and A. I. McNaught, "Spectral imaging of the retina," *Eye* **25**(3), 309–320 (2011).
32. L. E. MacKenzie and A. R. Harvey, "Oximetry using multispectral imaging: theory and application," *J. Opt.* **20**(6), 063501 (2018).
33. G. Carles, "Polarization-sensitive scattering in OpticStudio," <https://customers.zemax.com/os/resources/learn/knowledgebase/polarization-sensitive-scattering-in-opticstudio>. Accessed: 2018-10-13.
34. G. Carles, P. Zammit, and A. R. Harvey, "Holistic monte-carlo optical modelling of biological imaging," *Sci. Rep.* **9**(1), 15832 (2019).
35. A. N. Yaroslavsky, I. V. Yaroslavsky, T. Goldbach, and H.-J. Schwarzmaier, "Different phase-function approximations to determine optical properties of blood: a comparison," in *Optical Diagnostics of Biological Fluids and Advanced Techniques in Analytical Cytology*, vol. 2982 (1997).
36. M. Friebel, A. Roggan, G. J. Müller, and M. C. Meinke, "Determination of optical properties of human blood in the spectral range 250 to 1100 nm using monte carlo simulations with hematocrit-dependent effective scattering phase functions," *J. Biomed. Opt.* **11**(3), 034021 (2006).
37. A. N. Yaroslavsky, I. V. Yaroslavsky, T. Goldbach, and H.-J. Schwarzmaier, "Influence of the scattering phase function approximation on the optical properties of blood determined from the integrating sphere measurements," *J. Biomed. Opt.* **4**(1), 47–53 (1999).
38. N. Bosschaart, G. J. Edelman, M. C. G. Aalders, T. G. van Leeuwen, and D. J. Faber, "A literature review and novel theoretical approach on the optical properties of whole blood," *Lasers Med. Sci.* **29**(2), 453–479 (2014).
39. K. Briely-Sabo and A. B. A. Med, "Accurate de-oxygenation of ex vivo whole blood using sodium Dithionite," *Proc. Intl. Soc. Mag. Reson. Med.* **8**, 2025 (2000).
40. J. V. Kristjansdottir, S. H. Hardarson, A. R. Harvey, O. Olafsdottir, T. S. Eliasdottir, and E. Stefansson, "Choroidal Oximetry With a Noninvasive Spectrophotometric Oximeter," *Invest. Ophthalmol. Visual Sci.* **54**(5), 3234–3239 (2013).
41. S. Prahl, "Optical absorption of hemoglobin," <https://omlc.org/spectra/hemoglobin/> (1999). Accessed 2019-07-27.
42. D. J. Mordant, I. Al-Abboud, G. Muyo, A. Gorman, A. Sallam, P. Rodmell, J. Crowe, S. Morgan, P. Ritchie, A. R. Harvey, and A. I. McNaught, "Validation of human whole blood oximetry, using a hyperspectral fundus camera with a model eye," *Invest. Ophthalmol. Visual Sci.* **52**(5), 2851–2859 (2011).